Article

High activity and selectivity of single palladium atom for oxygen hydrogenation to H₂O₂

Shiming Yu [1], Xing Cheng[1], Yueshuai Wang[2], Bo Xiao[1], Yiran Xing[1], Jun Ren[3], Yue Lu [2], Hongyi Li [2] ✉, Chunqiang Zhuang [2] ✉ & Ge Chen [1] ✉

Nanosized palladium (Pd)-based catalysts are widely used in the direct hydrogen peroxide (H₂O₂) synthesis from H₂ and O₂, while its selectivity and yield remain inferior because of the O-O bond cleavage from both the reactant O₂ and the produced H₂O₂, which is assumed to have originated from various O₂ adsorption configurations on the Pd nanoparticles. Herein, single Pd atom catalyst with high activity and selectivity is reported. Density functional theory calculations certify that the O-O bond breaking is significantly inhibited on the single Pd atom and the O₂ is easier to be activated to form *OOH, which is a key intermediate for H₂O₂ synthesis; in addition, H₂O₂ degradation is shut down. Here, we show single Pd atom catalyst displays a remarkable H₂O₂ yield of 115 mol/g_{Pd}/h and H₂O₂ selectivity higher than 99%; while the concentration of H₂O₂ reaches 1.07 wt.% in a batch.

Hydrogen peroxide (H₂O₂) is one of the most important chemicals in industry, used in the production of fine chemicals and medicine, rocket fuels, sterilization, bleaching, and so on[1,2]. In the conventional process, H₂O₂ is mainly produced via the anthraquinone method, which consists of hydrogenation and oxidation of anthraquinone successively. The quest for an ecofriendly process for H₂O₂ synthesis is driven by the current disadvantages including high energy consumption and heavy pollution[3,4]. Under such circumstances, the direct synthesis of H₂O₂ from hydrogen (H₂) and oxygen (O₂) is an efficient and clean strategy to replace the anthraquinone oxidation process[5]. However, this process is challenging because of many parallel and consecutive reactions, as shown in Fig. 1. Specifically, compared to the synthesis of H₂O₂, it is thermodynamically more favorable to the production of H₂O via breaking O–O bonds, while the generated H₂O₂ also degrade through further hydrogenation and decomposition[6,7].

Palladium (Pd)[8,9] is a widely used catalyst in the direct synthesis of H₂O₂ due to its excellent hydrogenation activity. However, Pd is also active for side reactions and subsequent H₂O₂ degradation[10,11], resulting in an inferior H₂O₂ selectivity and poor yield. Pd-based nanoalloy catalyst (e.g., Pd-Pt, Pd-Au, Pd-Zn, Pd-Ag, Pd-Te, Pd-Sb, Pd-Sn)[5,12–23] can

effectively modify the electronic structure of Pd, thus inhibiting side reactions and H₂O₂ degradation. Besides, H₂O₂ can also be stabilized by adding strong acids or halides to the solvent, while it will cause metal shedding and needs a subsequent purification process to obtain pure H₂O₂[24,25]. Therefore, the rational design of a catalyst with high activity, high selectivity for oxygen hydrogenation to H₂O₂ as well as low degradation towards the generated H₂O₂ remains a formidable challenge.

The selectivity toward H₂O₂ is mainly determined by the competitive reactions between *OOH formation and O–O bond cleavage on catalysts which highly depend on the O₂ adsorption configuration[18,26–32]. The Pd nanoparticles involve various adsorption modes such as "side-on", "end-on" and "bridge", while the adsorption of O₂ on isolated Pd atom is usually the "end-on" type and could therefore reduce the possibility of O–O bond breaking. Thus, it would be encouraging to develop a single Pd atom catalyst to improve selectivity towards H₂O₂.

In this work, we have prepared a series of catalysts, among which the single Pd atom catalyst displays a remarkable H₂O₂ yield of 115 mol/g_{Pd}/h and a selectivity higher than 99%, surpassing the performance of

[1]Beijing Key Laboratory for Green Catalysis and Separation, Faculty of Environment and Life, Beijing University of Technology, Beijing 100124, P. R. China. [2]Faculty of Materials and Manufacturing, Beijing University of Technology, Beijing 100124, P. R. China. [3]North University of China, Taiyuan 030051, P. R. China. ✉e-mail: lhy06@bjut.edu.cn; chunqiang.zhuang@bjut.edu.cn; chenge@bjut.edu.cn

reported Pd-based catalysts. Besides, H_2O_2 degradation is also shut down, making it an ideal catalyst. The concentration of H_2O_2 reaches 1.07 wt.% in a batch. Density functional theory calculations reveal that the high yield and selectivity is believed to have originated from the high energy barrier of both O−O bond dissociation and H_2O_2 dissociation on the single Pd atom catalyst.

Results

Synthesis and characterization of materials

A series of TiO_2 (commercial P25)-supported O-Pd (oxidized Pd) catalysts were successfully synthesized through a simple hydrothermal method (Details in methods). For comparison, M-Pd (metallic Pd)/TiO_2 catalysts were also synthesized. Catalysts are named after the Pd loading. In the XRD pattern of O-Pd/TiO_2 samples (Fig. 2a and Supplementary Fig. 1a), there are no peaks associated with Pd species observed for 0.1% O-Pd/TiO_2 and 1% O-Pd/TiO_2, while a broad diffraction peak of PdO (101) around 34° appeared in 3% O-Pd/TiO_2 XRD

Fig. 1 | Schematic illustration in the direct synthesis of H_2O_2. all reactions in the direct synthesis of H_2O_2.

pattern. In contrast, the M-Pd/TiO_2 samples showed diffraction peaks of Pd (111) and Pd (200) around 40° and 46° except for 0.1%M-Pd /TiO_2 (Supplementary Fig. 1b), and the intensity of the peaks increased with the increase of palladium loading. XRD refinements results show that the lattice parameters of TiO_2 between samples are almost identical (Supplementary Fig. 1c−f), so the effect of different loading on the lattice of TiO_2 could be excluded. The catalyst morphology was further investigated by transmission electron microscopy (TEM) and aberration-corrected transmission electron microscopy (AC-TEM). No obvious Pd species can be seen from the TEM image of 0.1% O-Pd/TiO_2 (Supplementary Fig. 2a); however, single Pd atoms can be seen distributed over the TiO_2 by using AC-TEM (Fig. 2b). Because of the low z-contrast between Pd ($z = 46$) and Ti ($z = 22$), the single Pd atom in Fig. 2b may not be very clear. When the Pd loading reaches 1%, clusters were observed on the TiO_2, and the sizes are about 2 nm (Fig. 2c and Supplementary Fig. 2b). EDS mapping provided further evidence for a homogeneous distribution of Pd over the catalyst (Fig. 2d).

X-ray absorption spectroscopy (XAS) measurements were performed to probe the local environment of Pd atoms in O-Pd/TiO_2 and M-Pd/TiO_2. The X-ray absorption near edge structure (XANES) region of the XAS spectrum provides information about the oxidation state of Pd. The Pd K-edge absorption edge position for O-Pd/TiO_2 were like that of standard PdO sample (Fig. 3a), they were at higher photon energies than Pd metal, indicating that the Pd atoms in O-Pd/TiO_2 were in the oxidation state. Fourier transformed R-space curves of the Pd K-edge EXAFS spectra revealed the bonding environment of Pd species in O-Pd/TiO_2, an obvious peak at 1.75 Å was observed in the R-space spectrum of samples which was believed to be a Pd-O bond (Fig. 3b). The Pd metal foil and 1% M-Pd/TiO_2 showed an intense Pd-Pd feature at around 2.5 Å, which was absent in the O-Pd/TiO_2 samples (Fig. 3b), confirming that no Pd-Pd bonds were present in the O-Pd/TiO_2. And the fitting results showed the coordination number of Pd-O is 4 for 0.1% O-Pd/TiO_2 (Fig. 3c and
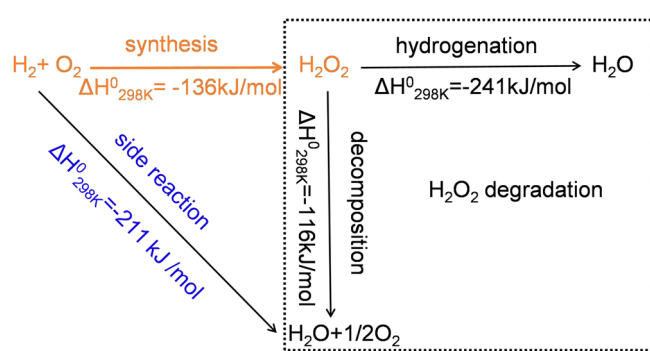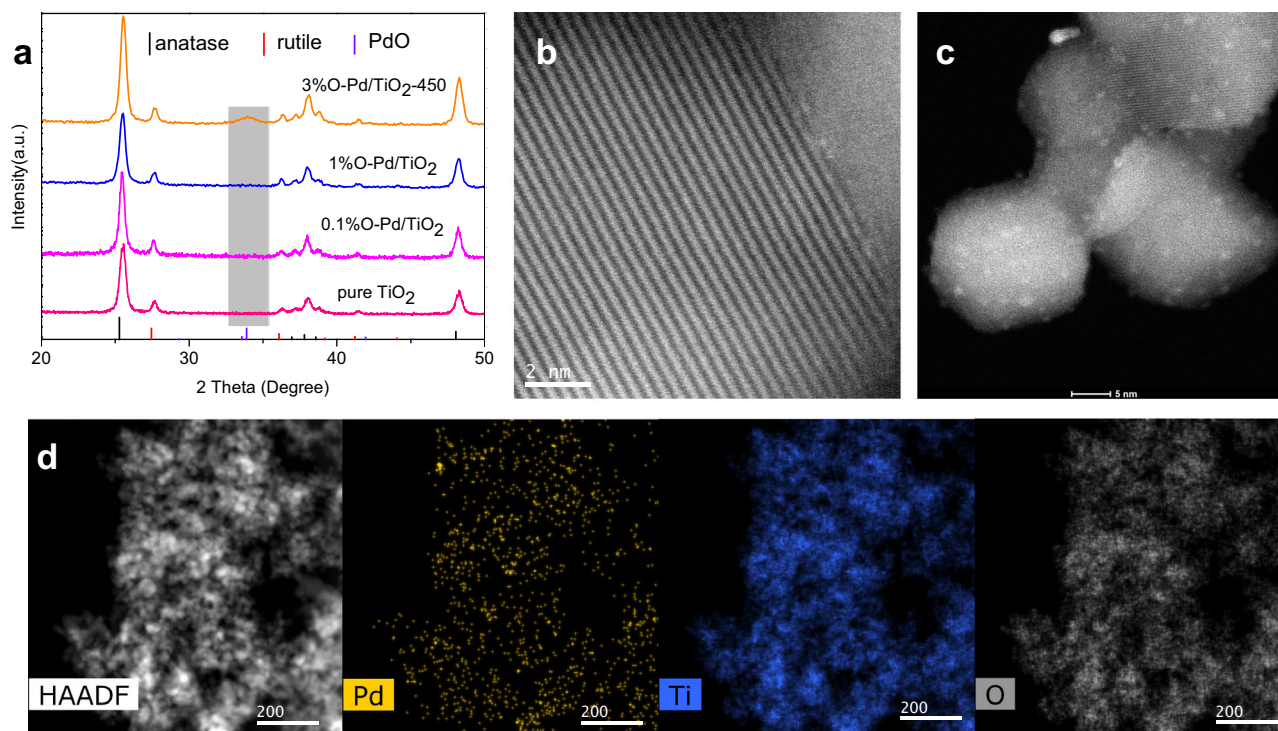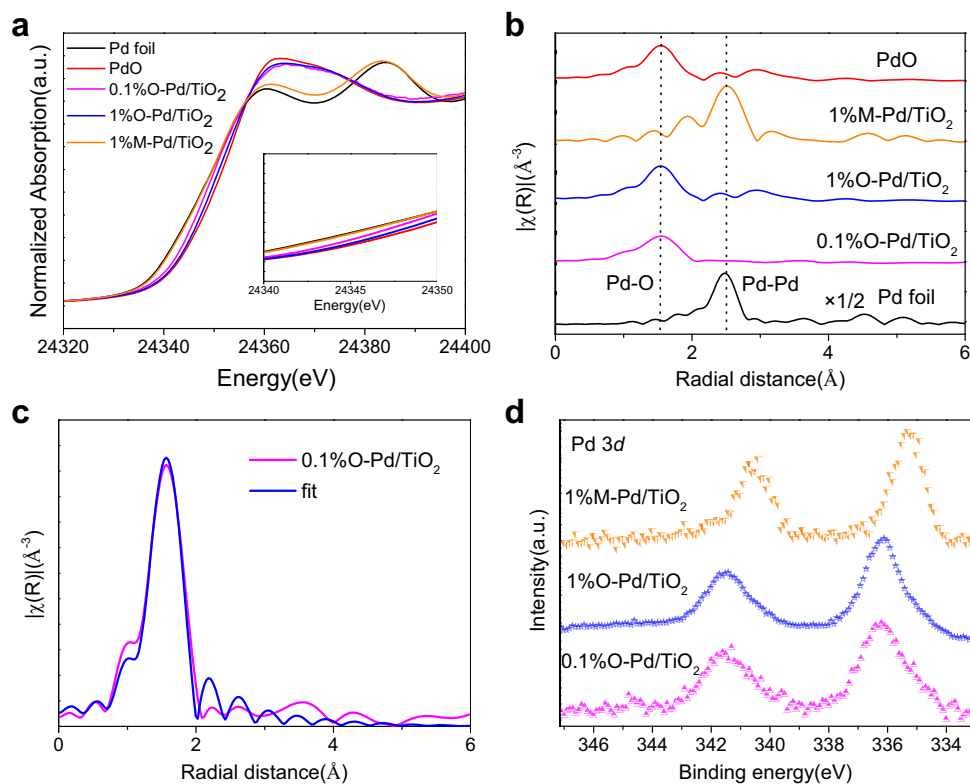

Fig. 2 | Structure characterization of the catalysts. a XRD patterns of O-Pd/TiO_2. **b** HAADF-STEM images of 0.1%O-Pd/TiO_2 with 2 nm scale bars. **c** HAADF-STEM images of 1% O-Pd/TiO_2 with 5 nm scale bars. **d** STEM-EDS elemental mappings 0.1% O-Pd/TiO_2, scale bars 200 nm.

Fig. 3 | Spectroscopic characterization. a XANES spectra at the Pd K-edge and **b** The Fourier transforms of Pd K-edge EXAFS spectra for catalysts, PdO, and Pd foil.

c The FT EXAFS fitting spectrum of 0.1% O-Pd/TiO$_2$ at R-space. **d** The X-ray photo-toelectron spectra of catalysts.

Supplementary Table 1), representative of the oxidized Pd single atoms on the surface of TiO$_2$[33,34]. These results confirmed that the Pd was atomically dispersed on TiO$_2$, which was consistent with the results of AC-TEM. The Pd K-edge absorption edge position and Fourier transformed R-space curves for M-Pd/TiO$_2$ were like Pd foil, indicating that the metallic Pd states in M-Pd/TiO$_2$ samples (Fig. 3a and Supplementary Fig. 3). X-ray photoelectron spectroscopy (XPS) analyses were presented in Fig. 3d, there is a strong signal of Pd^{2+} species (336.3 eV) in the spectra of 0.1% and 1% O-Pd/TiO$_2$. For M-Pd/TiO$_2$, we find that there is a strong signal of Pd^0 (334.9 eV) (Fig. 3d and Supplementary Fig. 4a). The absence of Cl peaks in the XPS spectra indicates that most of the chloride ions have been removed during the washing process, so the influence of chlorine ions on catalytic performance is excluded. (Supplementary Fig. 4b, c).

Catalytic performance. The O$_2$ hydrogenation to H$_2$O$_2$ was performed in a batch reactor with temperature at 2 °C controlled by an ice bath. We show that the catalytic performance of Pd catalysts in oxidation state (O-Pd/TiO$_2$) (including single Pd atom (0.1%), Pd cluster (1%)) are all better than that of metallic Pd catalyst (M-Pd/TiO$_2$). (Table 1, Entry 1–11). Particularly, the single Pd atom catalytic performance was up to 115 mol/kg$_{cat}$/h, and the selectivity of H$_2$O$_2$ was more than 99% (Table 1, Entry 1–2), which is superior to all other samples as well as the reported state-of-the-art catalysts (Table 1, Entry 1–2, 3–20). The Pd cluster catalyst (1% O-Pd/TiO$_2$) has a H$_2$O$_2$ yield of 79 mol/kg$_{cat}$/h, while the selectivity is 58% (Table 1, Entry 3–5), and the PdO nanoparticles demonstrate only a 7% selectivity to H$_2$O$_2$. For M-Pd/TiO$_2$, the H$_2$O$_2$ yield are much lower than that of O-Pd/TiO$_2$ (Table 1, Entry 8-11). For example, the H$_2$O$_2$ yield of 3% and 5% M-Pd/TiO$_2$ were 46 and 42 mol/kg$_{cat}$/h, respectively. Interestingly, the catalytic activity of 0.1% M-Pd/TiO$_2$ is very limited (Table 1, Entry8), as H$_2$O$_2$ yield was not detected. Also, we have synthesized 9% Pd/C catalyst, and the activity

and selectivity of Pd/C catalyst was inferior to both O-Pd/TiO$_2$ and M-Pd/TiO$_2$ catalysts. (Table 1, Entry 12).

Although the performance of the O-Pd/TiO$_2$ catalyst is superior to that of the M-Pd/TiO$_2$, whether the oxidized Pd species possessing high activity and selectivity remain controversial. The Burch et al. propose that M-Pd species has a higher activity and selectivity to H$_2$O$_2$[8]. Conversely, the Choudhary and Gaikwad et al. showed that oxidized Pd species exhibit better catalytic activity and selectivity by loading M-Pd and PdO on different oxide supports[25,35]. H$_2$ is easily activated on Pd^0 sites, while O$_2$ tends to be dissociated on successive Pd^0 sites; however, O$_2$ is stable on the surface of PdO[26]. Thus, both Pd^0 and Pd^{2+} species play vital roles in H$_2$O$_2$ synthesis. Recently, the DFT calculation by Wang et al. suggested that PdO (101) can effectively inhibit the dissociation of O−O bonds, leading to better activity and selectivity than Pd (111)[27], which is consistent with our experimental results.

The influence of reaction conditions (catalyst feeding and reaction time) on catalytic performance were further studied. For 0.1%O-Pd/TiO$_2$, the amount of H$_2$O$_2$ increases with the increase of catalyst feeding. For example, it can produce 144 μmol of H$_2$O$_2$ in half an hour when 2.5 mg 0.1%O-Pd/TiO$_2$ catalysts are fed, 10 mg can produce 390 μmol of H$_2$O$_2$ (78 mol/kg$_{cat}$/h), corresponding to 0.15% concentration (Fig. 4a), H$_2$ conversion is 10.43%, which is also comparable to PdSn catalysts (9% of H$_2$ conversion, 61 mol/kg$_{cat}$/h, 96% of selectivity) (Table 1, Entry 17). It is also noteworthy that the H$_2$O$_2$ selectivity of 0.1%O-Pd/TiO$_2$ is >99% regardless of the quantity of 2.5 mg, 5 mg, or 10 mg (Fig. 4b). On the contrary, for clusters and nanoparticles, the increase in the amount of H$_2$O$_2$ production is not obvious, but their H$_2$O$_2$ selectivity gradually decreases (Fig. 4a, b). Reaction time was extended from half an hour to three hours. We found that when the reaction time reached 2.5 h, the production of H$_2$O$_2$ was up to 1877 μmol (0.75% concentration) for 0.1%O-Pd/TiO$_2$ (Fig. 4c). However, when the reaction time is more than 2.5 h, the concentration of H$_2$O$_2$

Table 1 | Comparison of performance of the representative catalysts with our catalysts[a]

Entry	Catalyst	Pd loading (ICP-AES)	H_2O_2 yield (mol/kg_{cat}/h)	H_2O_2 yield (mol/g_{Pd}/h)	H_2O_2 degradation (mol/kg_{cat}/h)	H_2 conversion (100%)	H_2O_2 Selectivity (100%)	Ref.
Our results								
Oxidized								
1	0.05%O-Pd/TiO_2	0.05%	54	108	n.d.	1.84	> 99	–
2	0.1%O-Pd/TiO_2	0.1%	115	115	n.d.	3.85	> 99	–
3	0.5%O-Pd/TiO_2	0.5%	50	10	n.d.	4.31	40	–
4	1%O-Pd/TiO_2	1%	79	7.9	n.d.	4.70	58	–
5	2%O-Pd/TiO_2	1.5%	79	5.26	n.d.	5.44	50	–
6	3%O-Pd/TiO_2–450	2.7%	49	1.81	n.d.	7.67	22	–
7	3%O-Pd/ TiO_2–600	2.7%	23	0.85	n.d.	11.32	7	–
Metallic								
8	0.1%M-Pd/TiO_2	0.1%	n.d	n.d.	n.d.	n.d.	n.d.	
9	1%M-Pd/TiO_2	0.8%	61	7.62	518	4.89	43	–
10	3%M-Pd/TiO_2	2.7%	46	1.70	714	6.60	24	–
11	5%M-Pd/TiO_2	4.6%	42	0.91	867	10.33	14	–
12	9%Pd/C	9%	30	0.33	1054	25.83	4	–
Results in the literature								
13	Pd_5Zn/Al_2O_3	0.85%	216	25.431	177.54	56.6	78.5	[17]
14	0.5%Au/0.5% Pd/TiO_2	0.5%	99	19.8	230	–	70	
15	Pd_6Pb NRs/TiO_2-H-A	3.16%	170.1	5.667	260	40	56.7	[5]
16	2.5%Au-2.5%Pd/C	2.5%	110	4.4	n.d.	–	80	[4]
17	3 wt%Pd–2 wt% Sn/TiO_2	3%	61	2.03	n.d.	9	96	[23]
18	5 wt%Pd@NiO-3/TiO_2	5%	89	1.78	8	–	91	[16]
19	2.5%Au–2.5%Pd/C	2.5%	160	6.4	n.d.	–	>98	[22]
20	Pd_1Au_{220}	0.011%	–	–	–	–	95 ± 3	[30]

[a]H_2O_2 yield was determined under the following reaction conditions: 5% H_2/CO_2 (3.0 MPa) and 25% O_2/CO_2 (1.2 MPa), 8.5 g solvent (2.9 g water, 5.6 g CH_3OH), 2.5 mg catalyst, 2 °C, 1200 rpm, 30 min. H_2O_2 degradation was under standard reaction conditions: 5% H_2/CO_2 (3.0 MPa), 8.5 g solvent (5.6 g CH_3OH, 2.34 g H_2O, and 0.56 g 30% H_2O_2), 2.5 mg catalyst, 2 °C, 1200 rpm, 30 min. n. d., not detected. To ensure the reliability of the data, all the above experiments have to be tested for nine times, the data presented was the average value, the error of H_2O_2 yield and selectivity are within 1% and 4% respectively.

remains at 0.75%. The explanation might be that the large gas consumption in the reactor hinder the further generation of H_2O_2. To verify this point, we renew the gas in the reactor after the reaction of 2.5 h, and proceed with the reaction for the following 2.5 h (note the remaining gas in the reactor was completely discharged to 0 Mpa and then injected with 3.0 Mpa 5%H_2/CO_2 and 1.2 Mpa 25% O_2/CO_2). The results show that the concentration of H_2O_2 rose from 0.75% to 1.07% (2685 μmol). In general, H_2O_2 selectivity will decrease because of the side reactions and H_2O_2 degradation in a long-term reaction[8,23,24,31,32]. Interestingly, we found that the selectivity of 0.1%O-Pd/TiO_2 is always >99% no matter the reaction time (Fig. 4d). But for clusters and nanoparticles, the H_2O_2 selectivity does decline (Fig. 4d). One interpretation of this phenomenon is that as H_2 conversion increases, selectivity decreases due to H_2O_2 degradation. This can be better understood by comparing selectivity as a function of conversion for the different catalysts (Supplementary Fig. 5).

Therefore, we further measured the degradation rate of H_2O_2 under similar reaction conditions (3.0 Mpa 5%H_2/CO_2, the initial concentration of H_2O_2 is 2 wt.%). Firstly, the experiment shows that H_2O_2 does not degrade on TiO_2 support itself at 2 °C (Supplementary Table 2), which is consistent with the results previously reported by Edwards et al.[22]. Interestingly, the H_2O_2 degradation rate was not detected on the O-Pd/TiO_2 catalysts, but there was a significant H_2O_2 degradation rate on the M-Pd/TiO_2 catalysts; with the increase of metallic Pd loading, the degradation rate of H_2O_2 becomes higher

(Table 1, Supplementary Table 3). For example, the H_2O_2 degradation rate of 1% and 5%M-Pd/TiO_2 were 518 and 867 mol/kg_{cat}/h. To further understand the H_2O_2 degradation performance of catalysts, we have conducted a series of H_2O_2 degradation experiments under different conditions of atmosphere (5% H_2/CO_2 (3.0 MPa), 25% O_2/CO_2 (3.0 MPa) and pure N_2 (3.0 MPa), 5%H_2/N_2 (3.0 Mpa). (Supplementary Table 4).

Under the 5% H_2/CO_2 (3.0 MPa), the degradation of H_2O_2 was not detected on O-Pd/TiO_2 (Supplementary Table 4, Entry 1); to eliminate the influence of CO_2, we used 5% H_2/N_2 for the degradation experiment, the degradation rate was still not detected (Supplementary Table 4, Entry 8); however, the amount of H_2O_2 gradually decreased with time for M-Pd/TiO_2 catalyst. (Fig. 4e; Supplementary Table 4, Entry 2–3). On the other hand, we have not detected any degradation for both O-Pd/TiO_2 and M-Pd/TiO_2 catalyst under 25% O_2/CO_2 (3.0 MPa) or pure N_2 (3 Mpa). (Supplementary Table 4, Entry 4–7), which indicates the slow degradation of H_2O_2 in the absence of H_2. These observations suggested that the degradation rate of H_2O_2 is extremely low on the O-Pd/TiO_2 catalyst even in the presence of H_2. The result is meaningful for the degradation of H_2O_2 can be avoided without adding any inhibitors or pretreatment/post-treatment of catalysts.

Finally, we have investigated the stability of 0.1% O-Pd/TiO_2 catalyst (Fig. 4f) by measuring the H_2O_2 yield in the cycle test. The H_2O_2 yield decreased from 115 to 74 mol/kg_{cat}/h after reused five times. In the HAADF-STEM image of the used 0.1% O-Pd/TiO_2 (Supplementary
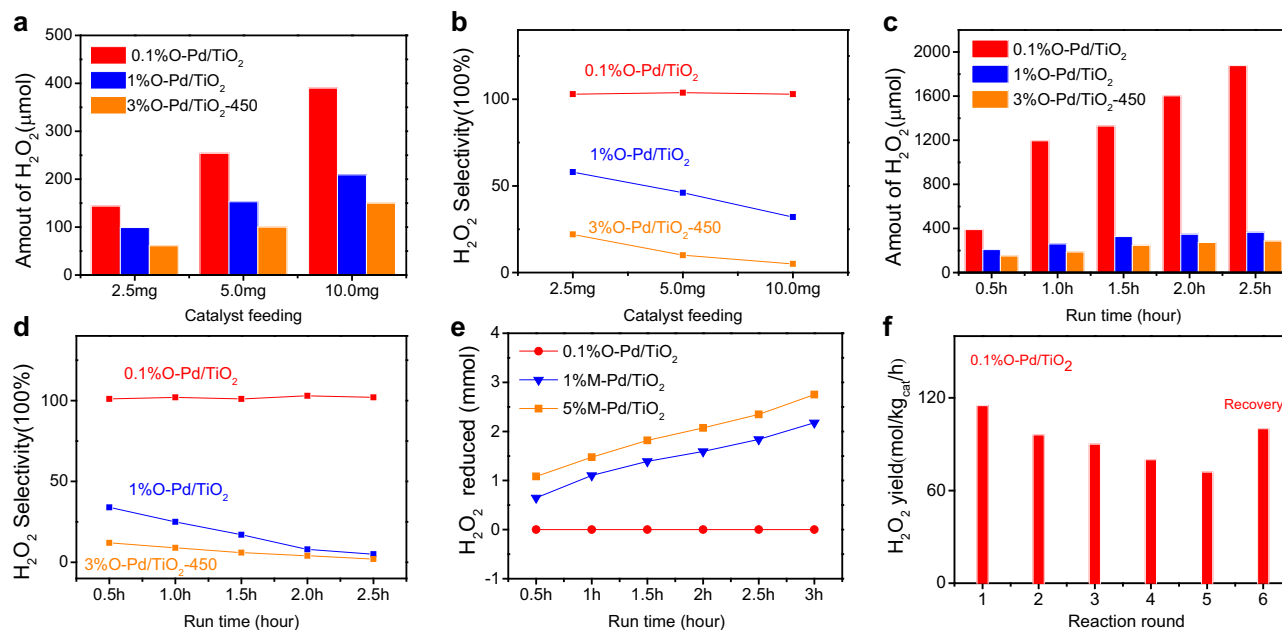
Fig. 4 | Catalytic performance. a, **b** The amounts of H_2O_2 and the H_2O_2 selectivity of different catalysts feeding. Reaction time: 30 min. **c**, **d** The amounts of H_2O_2 and the H_2O_2 selectivity of different reaction time. Catalyst feeding: 10 mg. **e** H_2O_2 degradation test. Reaction conditions: 5%H_2/CO_2 (3.0 Mpa), 2.5 mg of catalyst, 8.5 g solvent (2% H_2O_2),1200 rpm, 2 °C. **f** Stability test. Reaction conditions: 5%H_2/CO_2 (3.0 Mpa), 25%O_2/CO_2 (1.2 Mpa), 2.5 mg of catalyst, 8.5 g solvent, 1200 rpm, 2 °C, 30 min.

Fig. 6), we have observed some aggregated Pd species (about 3 nm Pd nanoparticle) on the TiO_2 particle by using EDS mapping, however, the homogenous distribution of Pd species in other places suggest that many single Pd atom still existed. The XPS results of the used catalyst reveal the existence of oxidized Pd species other than the metallic Pd species (Supplementary Figs. 7 and 8), which is consistent with the STEM result. Since the metallic Pd species showed very poor H_2O_2 yield in the experiment (Table 1, Entry 9–11), the observed Pd aggregation might mainly account for the loss of H_2O_2 yield in the recycle test. The decrease of H_2O_2 yield in the recycle experiment further indicates that the performance of the catalyst after reaction (co-existence of a single Pd atom and Pd nanoparticles) is not as good as that of the fresh catalyst, highlighting the important role of the initial single Pd (2+) state.

To further confirm this hypothesis, we have heated the used catalyst (after 5 cycles) at 350 °C for 3 h in the air, and the H_2O_2 yield increase from 74 mol/kg$_{cat}$/h to 100 mol/kg$_{cat}$/h, which is close to the fresh catalyst (Fig. 4f, round 6). It was also reported that the anneal treatment in the oxidative atmosphere will re-disperse the noble nanoparticle to a single noble metal atom on the oxide support[36–38]. Thus, it's reasonable to believe that the recovered H_2O_2 yield might be caused by the recovery of a single Pd^{2+} atom through annealing in the air, which also suggests the anneal treatment in the air is an effective method to refresh the used catalyst. The result again confirms that the single Pd^{2+} atom accounts for the high activity and selectivity towards the direct synthesis of H_2O_2.

Density functional theory calculations

As mentioned in the introduction section, the H_2O_2 selectivity is mainly determined by the competitive reactions between *OOH formation and O−O bond cleavage on catalysts. For these reasons, first-principles calculations are used to investigate the dissociation of O_2 and H_2O_2 over single atom and PdO clusters. Single Pd atom (Pd_1/TiO_2) and PdO clusters (Pd_8O_8/TiO_2) structure models were optimized on the surface of TiO_2 (101) (Supplementary Fig. 9). The Pd_1/TiO_2 model is based on the palladium-oxygen coordination number fitted by EXAFS, and Pd_8O_8 is extracted from the bulk phase of PdO, which simulates the

coordination information of Pd and O in large nanoparticles. It is shown that O_2 is adsorbed by "Pd-O-O" configuration on Pd_1/TiO_2 and is mainly adsorbed by "Pd-O-O-Pd" configuration on Pd_8O_8/TiO_2 (Supplementary Fig. 10). The oxidation state of Pd single atom estimated by bader charge analysis is (+1.73) between +1 and +2 (Supplementary Fig. 11), which is consistent with the XAS results.

Firstly, we have calculated the dissociation energy barrier of O_2 on Pd_1/TiO_2 and Pd_8O_8/TiO_2, respectively. The dissociation of O_2 on Pd_1/TiO_2 is a high energy process that is endothermic by 1.89 eV (Fig. 5a), while the dissociation energy barrier of O_2 on Pd_8O_8/TiO_2 needs only 1.08 eV, indicating that the dissociation of O_2 on Pd_1/TiO_2 is not favorable. And compared with the reported results of related DFT work (Supplementary Table 5), we find that the dissociation energy barrier of O−O bond on Pd_1/TiO_2 is the highest. This difference in the dissociation barrier can be attributed to structural differences (i.e., the adsorption configuration of oxygen on Pd). Oxygen can only be dissociated by migrating one oxygen atom to the nearby Ti site on Pd_1/TiO_2, whereas on Pd_8O_8/TiO_2 it can be directly fractured by "Pd-O-O-Pd" (Supplementary Fig. 12). Moreover, we found that H_2 is more easily activated on Pd_1/TiO_2 than Pd_8O_8/TiO_2 (Fig. 5b).

Similarly, the formation of *OOH on Pd_1/TiO_2 only needs to overcome the energy barrier of 0.81 eV, while Pd_8O_8/TiO_2 needs to overcome 1.25 eV (Fig. 5c). Structurally, the reason is that the adsorbed oxygen can directly capture the adsorbed hydrogen at the single Pd atom site, while clusters need to capture hydrogen from other Pd sites (Supplementary Fig. 13).

In addition, the reaction barriers for the step of OOH* hydrogenation to H_2O_2 and OOH* dissociation were investigated. On Pd_1/TiO_2, the formation of H_2O_2 only needs to cross an energy barrier of 0.16 eV, while OOH* dissociation needs to overcome 0.19 eV of barrier (Fig. 5d). In contrast, the formation of H_2O_2 needs to overcome 0.27 eV on Pd_8O_8/TiO_2, OOH* dissociation needs to overcome 0.35 eV of barrier (Fig. 5e). The calculated results suggest that Pd_1/TiO_2 is much more favorable than Pd_8O_8/TiO_2 for H_2O_2 formation.

The H_2O_2 degradation involved two steps (H_2O_2 → 2OH*; OH* + H* → H_2O). The calculated energy barrier of H_2O_2 dissociation into 2OH* on Pd_1/TiO_2 (0.58 eV) is higher than that of Pd_8O_8/TiO_2 (0.07 eV)
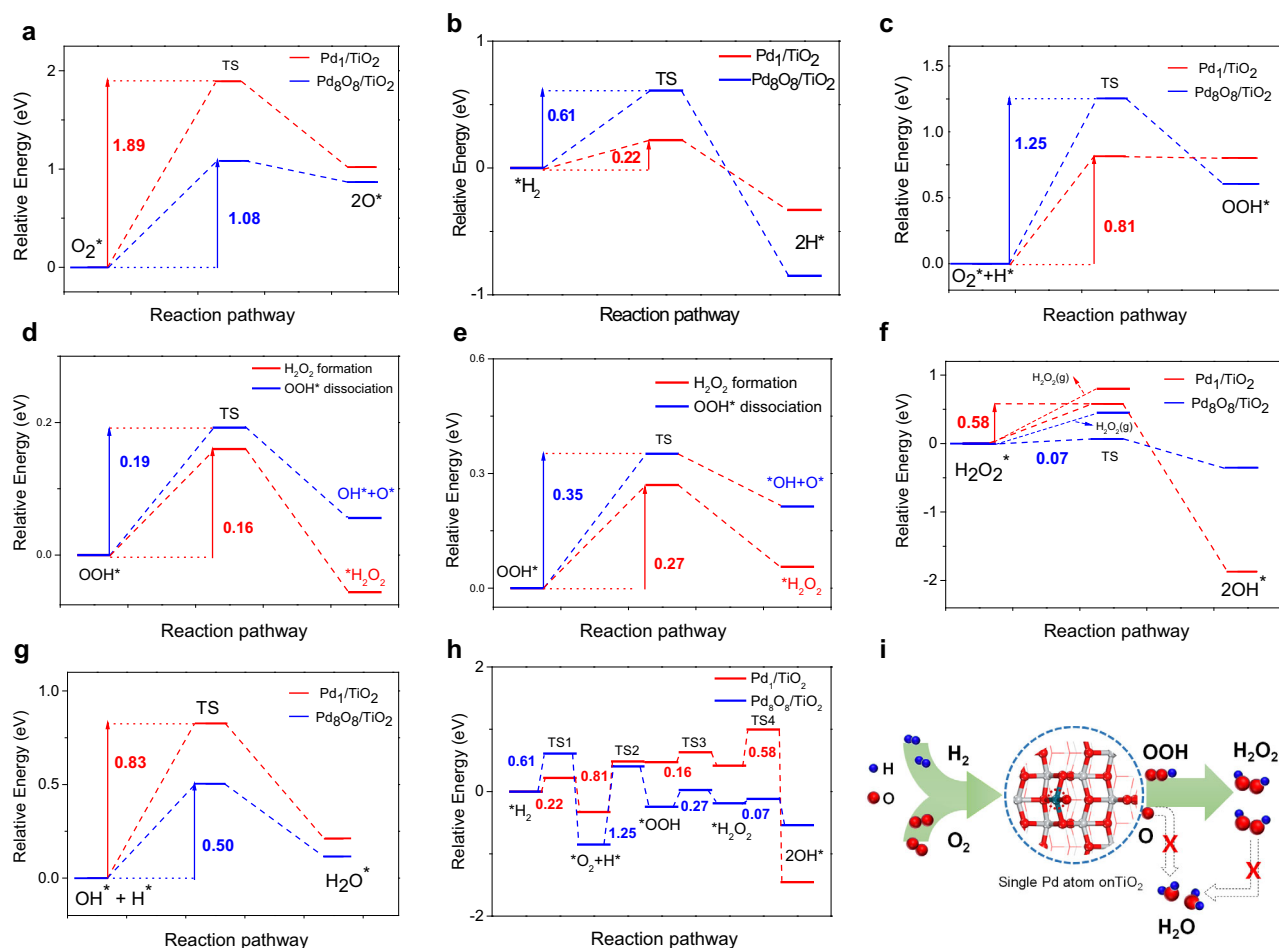
Fig. 5 | DFT calculations. a The reaction energy barriers of adsorbed *O_2 dissociation steps on Pd_1/TiO_2 and Pd_8O_8/TiO_2. **b** Energy profiles for H_2 dissociation on Pd_1/TiO_2 and Pd_8O_8/TiO_2. **c** The reaction energy barriers of adsorbed *O_2 hydrogenation steps on Pd_1/TiO_2 and Pd_8O_8/TiO_2. **d** The reaction energy barriers of H_2O_2 formation and OOH dissociation on Pd_1/TiO_2. **e** The reaction energy barriers of H_2O_2 formation and OOH dissociation on Pd_8O_8/TiO_2. **f** The reaction energy barriers of adsorbed H_2O_2* dissociation steps on Pd_1/TiO_2 and Pd_8O_8/TiO_2. **g** The reaction energy barriers of OH* with H* on Pd_1/TiO_2 and Pd_8O_8/TiO_2. **h** The entire reaction potential energy landscape on Pd_1/TiO_2 and Pd_8O_8/TiO_2. **i** Schematic illustration of H_2O_2 formation on single Pd atom catalyst.

(Fig. 5f), suggesting that H_2O_2 is more difficult to degrade on Pd_1/TiO_2. Moreover, the energy barrier of the reaction of the OH* with H* on Pd_1/TiO_2 (0.83 eV) is higher than that on the Pd_8O_8/TiO_2 (0.50 eV) (Fig. 5g). Therefore, after the calculation of these transition states, the entire reaction potential energy landscape can be obtained (Fig. 5h). The results reveal that it is conducive to the generation of H_2O_2 on Pd_1/TiO_2 than on Pd_8O_8/TiO_2, which is well consistent with the experimental observations. Therefore, a schematic diagram of H_2O_2 formation on single Pd atom catalyst is shown in Fig. 5i.

To sum up, the DFT calculation results confirm that single Pd atom catalysts favor the formation of the key intermediate (*OOH) and H_2O_2, but strongly suppress the cleavage of O−O bond in O_2 and OOH and H_2O_2, leading to a higher activity and selectivity. The calculation results also show that the different performances come from various adsorption configurations of O_2 on single atom and clusters at the beginning.

In summary, we have synthesized a series of O-Pd/TiO_2 (oxidized) and M-Pd/TiO_2 (metallic) catalysts for the oxygen hydrogenation to H_2O_2, the catalytic performance of O-Pd/TiO_2 (including single Pd atom (0.1%), Pd cluster (1%)) are all better than that of M-Pd/TiO_2 catalyst. Particularly, the single Pd atom catalyst displays ultrahigh activity (115 mol/g_{Pd}/h), which is 14 and 135 times higher than that of clusters and nanoparticles, respectively; and the selectivity to H_2O_2 is more than 99%. More interesting, H_2O_2 degradation was also shut down. The concentration of H_2O_2 reached 1.07 wt.% in a batch. DFT

calculations show that the O−O bond breaking is significantly inhibited on the single Pd atom and the O_2 is easier to be activated to form *OOH and H_2O_2; and the energy barrier of H_2O_2 degradation is also higher. As a result, the high yield and selectivity is obtained on single Pd atom catalyst. The work reports the application of single Pd atom catalysts in the direct synthesis of H_2O_2. We believe it will yield far-reaching implications for subsequent catalyst design in direct synthesis of H_2O_2 and corresponding mechanism research in the future.

Methods
Materials
Titanium (IV) oxide, Aeroxide P25 (Beijing Balinwei Technology Co., Ltd, product of Japan), Ethylene glycol (A.R. Tianjin Damao Chemical Reagent Factory), Na_2PdCl_4 (>36.0%, Annege Chemical). Methyl alcohol (G.R. Tianjin Guangfu Science and Technology Development Co., Ltd). Fe $(NH_4)_2 \cdot (SO_4)_2 \cdot 6H_2O$ (Tianjin Institute of Guangfu Fine Chemicals). Cerium sulfate (macklin reagent). Ultrapure water (18.2 MΩ cm). Stainless steel autoclave (Yanzheng Shanghai Instrument Co., Ltd). 5% H_2/CO_2, 5% H_2/N_2, pure N_2 and 25% O_2/CO_2 were purchased from Beijing Millennium Capital Gas Co. Ltd.

Synthesis of catalysts
Synthesis of O-Pd/TiO_2 (oxidized): TiO_2 was calcination at 450 °C for 4 h in the air (ramping rate: 5 °C/min) to remove surface water before catalysts preparation. The O-Pd/TiO_2 catalyst was

prepared using a hydrothermal synthesis method. The corresponding amount of Na_2PdCl_4 (10 g/L) was added to the TiO_2 (1 g) carrier suspension and heated to 80 °C for 3 h under magnetic stirring. Then, the obtained Pd/TiO_2 powder was centrifuged and freeze-dried overnight. Subsequently, the obtained catalyst was calcined at 350 °C for 3 h in the air at a heating rate of 5 °C/min. In order to obtain larger size palladium oxide nanoparticles, the samples with 3% palladium loading were heated at 450 °C and 600 °C for 3 h and other conditions remain unchanged. The prepared catalysts were denoted as 0.05%, 0.1%, 0.5%, 1%, 2% O-Pd/TiO_2 respectively according to the Pd loading. The catalysts with 3% Pd loading were labeled as 3% O-Pd/TiO_2−450 and 3% O-Pd/TiO_2−600, respectively, according to the calcination temperature.

Synthesis of M-Pd/TiO_2 (metallic): The preparation of M-Pd/TiO_2 was like that of O-Pd/TiO_2, except that the water was replaced with ethylene glycol and the temperature of TiO_2 carrier suspension was 100 °C, under reflux conditions. The catalysts were not calcined with air after centrifugally freeze-dried and used directly. The prepared catalysts were marked as 0.1,1,3, and 5% M-Pd/TiO_2 by the loading of palladium.

Characterization

The Pd loading on the catalysts was analyzed using an IRIS Intrepid ER/S (Thermo Elemental) inductively coupled plasma-atomic emission spectrometer (ICP-AES). Transmission electron microscopy (TEM) images were obtained using a Tecnai F20 microscope in conjunction with powder samples deposited onto a copper micro-grid and coated with carbon, applying an accelerating voltage of 200 kV. Spherical aberration corrected (Cs corrected) high angle annular dark field scanning transmission electron microscopy (HAADF-STEM) and energy-dispersive X-ray (EDX) mapping images were obtained with an FEI Titan G2 microscope equipped with a Super-X detector, operating at 300 kV. X-ray diffraction (XRD) patterns of the samples were recorded on a Bruker D8 Advance system with Cu Kα radiation at 40 kV and 40 mA. X-ray photoelectron spectroscopy (XPS) analyses were performed using a Kratos Axis Ultra XPS spectrometer with monochromatized Al-Kα radiation and an energy resolution of 0.48 eV. The X-ray absorption fine structure (XAFS) spectrum data were collected on the BL14W1 beamline radiation equipment of the Shanghai Synchrotron Radiation Facility (SSRF) of the Shanghai Institute of Applied Physics (SINAP). Pd foil, PdO samples were used as references. All target samples and references were measured by fluorescence or transmission mode. Extended X-ray adsorption fine structure (EXAFS) fitting was conducted using the software of Artemis.

Catalytic experimental measurement

Catalytic experiments were operated using a stainless-steel autoclave with a nominal volume of 50 mL and a maximum working pressure of 14 MPa.

H_2O_2 synthesis. In the typical experiment of H_2O_2 synthesis, 2.5 mg catalyst and 8.5 g solvent (5.6 g CH_3OH (HPLC grade), 2.9 g H_2O) were added into the autoclave. Before 3.0 MPa 5%H_2/CO_2 was injected at room temperature, the reactor was purged three times with 0.7 MPa (5%H_2/CO_2), then the temperature was reduced to 2 °C (in an ice bath), the pressure was about 2.3 MPa, at this time, 1.2 MPa 25% O_2/CO_2 was injected, and the total pressure was 3.5 MPa. Temperature and pressure are respectively detected by thermocouple and pressure sensor. The stirring speed was controlled at 1200 rpm.

The H_2O_2 yield was detected by acidified Ce $(SO_4)_2$ (0.01 M) titration in the presence of two drops of ferroin indicator. The Ce $(SO_4)_2$ solutions were standardized against $(NH_4)_2Fe(SO_4)_2\cdot6H_2O$ using ferroin as an indicator. Catalyst yields are marked as mol H_2O_2 $kg_{cat}^{-1}h^{-1}$

according to the following equation.

$$H_2O_2 \text{ Yield} = (\text{moles of } H_2O_2 \text{ generated})/(\text{mass of catalyst} \times \text{time}) \quad (1)$$

Gas analysis was performed by gas chromatography (GC-2020) equipped with a TDX-01 column connected to a thermal conductivity detector. Conversion of H_2 was calculated by gas analysis before and after the reaction. H_2O_2 selectivity was calculated according to the following equation:

$$H_2O_2 \text{ Selectivity} = (\text{moles of } H_2O_2 \text{ generated})/(\text{mass of } H_2 \text{ reacted}) \times 100\%$$
$$(2)$$

H_2O_2 degradation. The experiments were manipulated in a similar way to the H_2O_2 synthesis, but in the absence of 1.2 MPa 25%O_2/CO_2. In detail, H_2O from the 8.5 g of solvent was replaced by a 30% H_2O_2 solution to give a reaction solvent containing between 2-8 wt%H_2O_2. The standard reaction conditions adopted for H_2O_2 degradation were as follows: 2.5 mg catalyst, 8.5 g solvent (5.6 g CH_3OH, 2.34 g H_2O, and 0.56 g 30% H_2O_2, 3.0 MPa 5%H_2/CO_2, 2 °C, 1200 rpm, 30 min). The H_2O_2 degradation rate is a combination of H_2O_2 hydrogenation and decomposition. H_2O_2 degradation rate was calculated following:

$$H_2O_2 \text{ degradation rate} = (\text{moles of } H_2O_2 \text{ reduced})/(\text{mass of catalyst} \times \text{time})$$
$$(3)$$

To ensure the reliability of the data, all the above experiments have to be tested for nine times, the data presented was the average value, the error of H_2O_2 yield and selectivity are within 1%, 4% respectively.

Calculation details

All the spin-polarized density functional (DFT) calculations were carried out with the Vienna Ab initio Simulation Package(VASP)[39]. The ion-electron interaction was described by the projector augmented wave (PAW) method[40]. The generalized gradient approximation (GGA) in the Perdew-Burke-Ernzerhof (PBE) functional was used for the exchange-correlation interactions[41]. The DFT-D3 method was introduced to describe van der Waals interactions[42]. The 15 Å vacuum slab in the z direction was applied to avoid interactions with adjacent units. The cut-off energy for plane-wave basis set was 450 eV. The convergence criterion for energy and force were set as 10-5 eV and 0.03 eV/Å during geometry optimization, respectively. The Brillouin zone was sampled with $2 \times 2 \times 1$ k-point grids. Transition states were located with the climbing-image nudged elastic band (CI-NEB) method[43], and the threshold value for the forces on each atom was 0.05 eV/Å.

Data availability

The data supporting this study are available within the paper and the Supplementary Information. All other relevant source data are available from the corresponding authors upon reasonable request. Source data are provided with this paper.

References

1. Bryliakov, K. P. Catalytic asymmetric oxygenations with the environmentally benign oxidants H_2O_2 and O_2. *Chem. Rev.* **117**, 11406–11459 (2017).
2. Campos-Martin, J. M., Blanco-Brieva, G. & Fierro, J. L. G. Hydrogen peroxide synthesis: an outlook beyond the anthraquinone process. *Angew. Chem. Int. Ed.* **45**, 6962–6984 (2006).
3. Zhou, Y., Chen, G. & Zhang, J. A review of advanced metal-free carbon catalysts for oxygen reduction reactions towards the selective generation of hydrogen peroxide. *J. Mater. Chem. A* **8**, 20849–20869 (2020).

4. Edwards, J. K. & Hutchings, G. J. Palladium and gold-palladium catalysts for the direct synthesis of hydrogen peroxide. *Angew. Chem. Int. Ed.* **47**, 9192–9198 (2008).

5. Cao, K. et al. Efficient Direct H_2O_2 Synthesis Enabled by PdPb Nanorings via Inhibiting the O–O Bond Cleavage in O_2 and H_2O_2. *ACS Catal.* **11**, 1106–1118 (2021).

6. Lari, G. M. et al. Hybrid palladium nanoparticles for direct hydrogen peroxide synthesis: the key role of the ligand. *Angew. Chem. Int. Ed.* **56**, 1775–1779 (2017).

7. Flaherty, D. W. Direct synthesis of H_2O_2 from H_2 and O_2 on Pd catalysts: current understanding, outstanding questions, and research needs. *ACS Catal.* **8**, 1520–1527 (2018).

8. Burch, R. & Ellis, P. R. An investigation of alternative catalytic approaches for the direct synthesis of hydrogen peroxide from hydrogen and oxygen. *Appl. Catal. B* **42**, 203–211 (2003).

9. Solsona, B. E. et al. Direct synthesis of hydrogen peroxide from H_2 and O_2 using Al_2O_3 supported Au-Pd catalysts. *Chem. Mater.* **18**, 2689–2695 (2006).

10. Han, G., Lee, S., Hwang, S. & Lee, K. Advanced development strategy of nano catalyst and DFT calculations for direct synthesis of hydrogen peroxide. *Adv. Energy Mater.* **11**, 2003121 (2021).

11. Edwards, J. K. et al. Strategies for designing supported gold-palladium bimetallic catalysts for the direct synthesis of hydrogen peroxide. *Acc. Chem. Res.* **47**, 845–854 (2014).

12. Fumin, L. et al. Hollow Pd–Sn nanocrystals for efficient direct H_2O_2 synthesis: the critical role of Sn on structure evolution and catalytic performance. *ACS Catal.* **8**, 3418–3423 (2018).

13. Zhang, J. et al. Highly active, selective, and stable direct H_2O_2 generation by monodispersive Pd–Ag nanoalloy. *ACS Appl. Mater. Inter.* **10**, 21291–21296 (2018).

14. Wilson, N. M. et al. Direct synthesis of H_2O_2 on AgPt octahedra: the importance of Ag–Pt coordination for high H_2O_2 selectivity. *ACS Catal.* **8**, 2880–2889 (2018).

15. Han, G. et al. Tailored palladium–platinum nanoconcave cubes as high performance catalysts for the direct synthesis of hydrogen peroxide. *ACS Appl. Mater. Inter.* **12**, 6328–6335 (2020).

16. Feng, Y. et al. Surface engineering at the interface of core/shell nanoparticles promotes hydrogen peroxide generation. *Natl Sci. Rev.* **5**, 895–906 (2018).

17. Wang, S. et al. Effect of Zn addition on the direct synthesis of hydrogen peroxide over supported palladium catalysts. *Appl. Catal. A* **531**, 89–95 (2017).

18. Wilson, N. M. et al. Direct synthesis of H_2O_2 on PdZn nanoparticles: the impact of electronic modifications and heterogeneity of active sites. *J. Catal.* **368**, 261–274 (2018).

19. Tian, P. et al. Revealing the role of tellurium in palladium-tellurium catalysts for the direct synthesis of hydrogen peroxide. *J. Catal.* **385**, 21–29 (2020).

20. Ding, D. et al. Promotional effects of Sb on Pd-based catalysts for the direct synthesis of hydrogen peroxide at ambient pressure. *Chin. J. Catal.* **39**, 673–681 (2018).

21. Jennifer, K. E. et al. Direct synthesis of hydrogen peroxide from H_2 and O_2 using Au-Pd/Fe_2O_3 catalysts. *J. Mater. Chem.* **236**, 69–79 (2005).

22. Jennifer, K. E. et al. Switching off hydrogen peroxide hydrogenation in the direct synthesis process. *Science* **323**, 1037–1041 (2009).

23. Freakley, S. J. et al. Palladium-tin catalysts for the direct synthesis of H_2O_2 with high selectivity. *Science* **351**, 965–968 (2016).

24. Zhu, J. et al. Direct synthesis of pure aqueous H_2O_2 solution within aluminosilicate zeolite crystals. *ACS Catal.* **11**, 1946–1951 (2021).

25. Choudhary, V. R. et al. Direct oxidation of H_2 to H_2O_2 over Pd-based catalysts: influence of oxidation state, support and metal additives. *Appl. Catal. A-gen.* **308**, 128–133 (2006).

26. Pengfei, T. et al. The origin of palladium particle size effects in the direct synthesis of H_2O_2: Is smaller better. *J. Catal.* **349**, 30–40 (2017).

27. Fang, W. et al. How does the oxidation state of palladium surfaces affect the reactivity and selectivity of direct synthesis of hydrogen peroxide from hydrogen and oxygen gases? A density functional study. *J. Am. Chem. Soc.* **141**, 901–910 (2019).

28. Wilson, N. M. et al. Mechanism for the direct synthesis of H_2O_2 on Pd clusters: heterolytic reaction pathways at the liquid-solid interface. *J. Am. Chem. Soc.* **138**, 574–586 (2016).

29. Wilson, N. M. et al. Direct synthesis of H_2O_2 on Pd and Au_xPd_1 clusters: understanding the effects of alloying Pd with Au. *J. Catal.* **357**, 163–175 (2018).

30. Tomas, R. et al. Effect of Pd coordination and isolation on the catalytic reduction of O_2 to H_2O_2 over PdAu bimetallic nanoparticles. *J. Am. Chem. Soc.* **143**, 5445–5464 (2021).

31. Chinta, S. & Lunsford, J. H. A mechanistic study of H_2O_2 and H_2O formation from H_2 and O_2 catalyzed by palladium in an aqueous medium. *J. Catal.* **225**, 249–255 (2004).

32. Lunsford, J. H. The direct formation of H_2O_2 from H_2 and O_2 over palladium catalysts. *J. Catal.* **216**, 455–460 (2003).

33. Liu, P. et al. Photochemical route for synthesizing atomically dispersed palladium catalysts. *Science* **352**, 797–801 (2016).

34. Liu, P. et al. Photochemical route for preparing atomically dispersed Pd_1/TiO_2 catalysts on (001)-exposed anatase nanocrystals and P25. *Chin. J. Catal.* **38**, 1574–1580 (2017).

35. Gaikwad, A. G. et al. Direct oxidation of hydrogen to hydrogen peroxide over Pd-containing fluorinated or sulfated Al_2O_3, ZrO_2, CeO_2, ThO_2, Y_2O_3 and Ga_2O_3 catalysts in stirred slurry reactor at ambient conditions. *J. Mol. Catal. A Chem.* **181**, 143–149 (2002).

36. Camellone, M. F. et al. Adatom and nanoparticle dynamics on single-atom catalyst substrates. *ACS Catal.* **12**, 4859–4871 (2022).

37. Liu, S. et al. Identify the activity origin of Pt single-atom catalyst via atom-by-atom counting. *J. Am. Chem. Soc.* **143**, 15243–15249 (2021).

38. Doherty, F. et al. Nanocluster and single-atom catalysts for thermocatalytic conversion of CO and CO_2. *Catal. Sci. Technol.* **10**, 5772–5791 (2020).

39. Furthmüller, K. G. Efficiency of ab-initio total energy calculations for metals and semiconductors using a plane-wave basis set. *Comp. Mater. Sci.* **6**, 15–50 (1996).

40. Blöchl, P. E. Projected augmented-wave method. *Phys. Rev. B* **50**, 17953–17979 (1994).

41. Perdew, J. P. et al. Erratum: Atoms, molecules, solids, and surfaces: Applications of the generalized gradient approximation for exchange and correlation. *Phys. Rev. B* **46**, 6671–6687 (1992).

42. S. Grimme, J. et al. A consistent and accurate ab initio parametrization of density functional dispersion correction (DFT-D) for the 94 elements H-Pu. *Chem. Phys.* **132**, 154104 (2010).

43. Henkelman, G., Uberuaga, B. P. & Jónsson, H. Alchemical derivatives of reaction energetics. *Chem. Phys.* **113**, 9901–9904 (2000).

Acknowledgements

Author contributions

S.Y. Conceptualization, Methodology, Investigation, Writing-original draft. X.C. Validation, Formal analysis, Data curation. Y.W. Validation,

Data curation. B.X. Data curation. Y.X. Validation, Formal analysis. J.R. DFT calculation. Y.L. Data curation. H.L. Resources, Data curation. C.Z. Writing—review and editing. G.C. Writing—review and editing, Supervision.

Competing interests

Additional information